

# Structure of HsdS Subunit from *Thermoanaerobacter tengcongensis* Sheds Lights on Mechanism of Dynamic Opening and Closing of Type I Methyltransferase

Pu Gao<sup>1,2</sup>, Qun Tang<sup>1</sup>, XiaoMin An<sup>1</sup>, XiaoXue Yan<sup>1\*</sup>, DongCai Liang<sup>1\*</sup>

**1** National Laboratory of Biomacromolecules, Institute of Biophysics, Chinese Academy of Sciences, Beijing, China, **2** Graduate University of Chinese Academy of Sciences, Beijing, China

## Abstract

Type I DNA methyltransferases contain one specificity subunit (HsdS) and two modification subunits (HsdM). The electron microscopy model of M.EcoKI-M<sub>2</sub>S<sub>1</sub> methyltransferase shows a reasonable closed state of this clamp-like enzyme, but the structure of the open state is still unclear. The 1.95 Å crystal structure of the specificity subunit from *Thermoanaerobacter tengcongensis* (TTE-HsdS) shows an unreported open form inter-domain orientation of this subunit. Based on the crystal structure of TTE-HsdS and the closed state model of M.EcoKI-M<sub>2</sub>S<sub>1</sub>, we constructed a potential open state model of type I methyltransferase. Mutational studies indicated that two  $\alpha$ -helices (aa30-59 and aa466-495) of the TTE-HsdM subunit are important inter-subunit interaction sites in the TTE-M<sub>2</sub>S<sub>1</sub> complex. DNA binding assays also highlighted the importance of the C-terminal region of TTE-HsdM for DNA binding by the TTE-M<sub>2</sub>S<sub>1</sub> complex. On the basis of structural analysis, biochemical experiments and previous studies, we propose a dynamic opening and closing mechanism for type I methyltransferase.

**Citation:** Gao P, Tang Q, An X, Yan X, Liang D (2011) Structure of HsdS Subunit from *Thermoanaerobacter tengcongensis* Sheds Lights on Mechanism of Dynamic Opening and Closing of Type I Methyltransferase. PLoS ONE 6(3): e17346. doi:10.1371/journal.pone.0017346

**Editor:** Wenqing Xu, University of Washington, United States of America

**Received:** October 29, 2010; **Accepted:** January 29, 2011; **Published:** March 2, 2011

**Copyright:** © 2011 Gao et al. This is an open-access article distributed under the terms of the Creative Commons Attribution License, which permits unrestricted use, distribution, and reproduction in any medium, provided the original author and source are credited.

**Funding:** This study was supported by grants from the National Program on Key Basic Research Project "973 Program" No. 2007CB914302, No. 2011CB966303, No. 2011CB910302 and No. 2011CB911101. Additional support was provided by the National Natural Science Foundation of China, No. 30600102 and No. 31070684. Funding for open access charge: Institute of Biophysics, Chinese Academy of Sciences. The funders had no role in study design, data collection and analysis, decision to publish, or preparation of the manuscript.

**Competing Interests:** The authors have declared that no competing interests exist.

\* E-mail: snow@moon.ibp.ac.cn (XXY); dcliang@sun5.ibp.ac.cn (DCL)

## Introduction

Restriction-modification (R-M) systems maintain the integrity of bacterial genomes by cleaving foreign DNA [1]. Four types of R-M enzymes are presently known: I, II, III, and IV [2,3]. The most complex of the four enzymes is the type I enzyme which is also the first R-M enzyme discovered [4]. Type I R-M enzymes are composed of three different subunits: a specificity subunit (HsdS or S) that recognizes specific DNA sequences, a methylation subunit (HsdM or M) that methylates target adenine bases, and a restriction subunit (HsdR or R) that translocates from the recognition site and cleaves DNA at variable positions [2,5]. The HsdS subunit consists of two globular domains that correspond to the variable target recognition domains (TRD1 and TRD2) and two conserved regions (CR1 and CR2) that separate the TRDs. The three subunits can assemble into two types of complexes: R<sub>2</sub>M<sub>2</sub>S<sub>1</sub> with both methyltransferase and restrictase activities, or M<sub>2</sub>S<sub>1</sub> with only methyltransferase activity [6]. M<sub>2</sub>S<sub>1</sub> is also the core DNA-binding component of the R-M enzyme [7]. Together, the M<sub>2</sub>S<sub>1</sub> complex recognizes an asymmetric, bipartite nucleotide target containing two specific regions 3 to 5 bp in length that are separated by nonspecific DNA sequences of 6 to 8 bp [8,9].

The orientation of the TRDs and the CRs are quite different between the two published structures for the HsdS subunit (Mja-HsdS [10] and Mge-HsdS [6]). The difference in observed

structures suggests that domain motion occurs within the HsdS subunit [7,11,12]. However, the structural basis of the inter-domain movements has not been established. Domain motion within the HsdS subunit might result in conformational changes and dynamic opening and closing of the whole M<sub>2</sub>S<sub>1</sub> complex [13]. The electron microscopy (EM) model of M.EcoKI-M<sub>2</sub>S<sub>1</sub> fits a closed state type I methyltransferase [13], but does not provide clear information about the open state. Crystal structures of Mja-HsdS [10] and Mge-HsdS [6] based on the mode of inter-subunit interactions in the M.EcoKI-M<sub>2</sub>S<sub>1</sub> EM model and the domain orientation of the HsdS subunit cannot result in an open form of the M<sub>2</sub>S<sub>1</sub> complex. An open state model of the M<sub>2</sub>S<sub>1</sub> complex is needed in order to understand the structure of the complex and to model the dynamic opening and closing of the complex. Three dimensional structures of the HsdS subunit with an open form domain-orientation are therefore needed.

The EM model of M.EcoKI-M<sub>2</sub>S<sub>1</sub> reveals that the N terminal domains of the two HsdM subunits contact each other, while the C terminal domain of the HsdM subunits contact the HsdS subunit [13]. Other studies indicate that the C terminal region of the HsdM subunit is essential for the assembly of the EcoKI methyltransferase [14], while mutation in the N terminal domain of the HsdM subunit reduces the affinity of the enzyme for hemimethylated targets [15,16]. There are two possible HsdS-HsdM interfaces in HsdS subunit. One possible interface is the connection region between CRs and TRDs [10,13,17]. The other

possible interface is at a helix-loop structure in the TRDs [13]. Until now, the exact sites of interaction at the HsdM-HsdS and HsdM-HsdM interfaces have not been identified.

We report here the crystal structure of HsdS from *Thermoanaerobacter tengcongensis* in an open form conformation at 1.95 Å resolution. Based on structural comparisons and modelling, we propose a hemi-open state model for the M<sub>2</sub>S<sub>1</sub> complex. Also, mutational studies were used to reveal the inter-subunit interaction sites of type I methyltransferases from *T. tengcongensis* (TTE-M<sub>2</sub>S<sub>1</sub>). Based on the structural and mutational evidence presented here, we have supposed a dynamic “opening and closing” way of the M<sub>2</sub>S<sub>1</sub> complex.

## Materials and Methods

### Cloning and vector construction

The *tte-hsdS* and *tte-hsdM* gene were amplified by PCR from *T. tengcongensis* genomic DNA [18]. The PCR products of *tte-hsdS* (ORF: TTE1545) and *tte-hsdM* (ORF: TTE1547) were cloned into the pET-DUET co-expression vector at cloning sites 1 (with N-terminal His tag) and 2 (without tag) respectively. Based on this co-expression vector of “wild type TTE-HsdS/wild type TTE-HsdM”, we also constructed several co-expression vectors of “wild type TTE-HsdS/mutant TTE-HsdM”. Details of these co-expression vectors are summarized in **Table 1**. An expression vector of TTE-HsdS alone was also constructed by cloning the PCR product of *tte-hsdS* into the pHAT-2 expression vector.

### Protein expression and purification

All vectors were transformed into BL21 (DE3) *Escherichia coli* cells. The cells were grown in LB media supplemented with 100 mg/mL ampicillin until they reached log phase growth (OD<sub>600</sub> = 0.6). The expression of TTE-HsdS was induced by stimulation with IPTG (0.4 mM) at 28°C for 10 h. Cells were harvested and resuspended in buffer A (20 mM HEPES pH 7.0, 300 mM NaCl, 5% glycerol, 3 mM β-mercaptoethanol) and then lysed by sonication. The lysate was clarified by centrifugation and purified by passage through a nickel-affinity column. A further purification step was then performed using size exclusion chromatography on a Superdex 200 column (Amersham). The

purified protein was concentrated to 15 mg/mL for crystallization in buffer B (5 mM HEPES pH 7.0, 300 mM NaCl, 5% glycerol, 1 mM DTT). A number of TTE-HsdS/TTE-HsdM complexes were expressed and purified using the same protocol.

### Crystallization and data collection

Crystals of recombinant TTE-HsdS were grown at 20°C using the hanging-drop, vapor-diffusion method. Drops consisted of 2 μL of protein solution and 2 μL of mother liquor (0.1 M Bis-Tris pH 6.4, 1.16 M (NH<sub>4</sub>)<sub>2</sub>SO<sub>4</sub>). Crystals suitable for X-ray diffraction studies were obtained after 5 days growth. Hg derivatives were obtained using the same protocol as in our previous work [19]. Native and derivative crystals were soaked in 2 M Li<sub>2</sub>SO<sub>4</sub> for 2 min before data collection and were flash-frozen in liquid nitrogen. Native crystal data were collected on a beamline NW12A (Photon Factory, KEK, Japan). Derivative data were collected on a Rigaku FR-E X-ray generator with a Rigaku R-Axis IV++ image plate detector. Data were integrated and scaled with HKL2000 [20]. Statistical analysis of the data collected is summarized in **Table 2**.

**Table 1.** Co-expression vectors of TTE-HsdS and TTE-HsdM.

Vectors	MCS1	MCS2
petDUET_SM	TTE-HsdS (wild type)	TTE-HsdM (wild type)
petDUET_SM <sub>Δn10</sub>	TTE-HsdS (wild type)	TTE-HsdM (aa001-010 deletion)
petDUET_SM <sub>Δn30</sub>	TTE-HsdS (wild type)	TTE-HsdM (aa001-030 deletion)
petDUET_SM <sub>Δn40</sub>	TTE-HsdS (wild type)	TTE-HsdM (aa001-040 deletion)
petDUET_SM <sub>Δn50</sub>	TTE-HsdS (wild type)	TTE-HsdM (aa001-050 deletion)
petDUET_SM <sub>Δc10</sub>	TTE-HsdS (wild type)	TTE-HsdM (aa498-507 deletion)
petDUET_SM <sub>Δc21</sub>	TTE-HsdS (wild type)	TTE-HsdM (aa487-507 deletion)
petDUET_SM <sub>Δc30</sub>	TTE-HsdS (wild type)	TTE-HsdM (aa478-507 deletion)
petDUET_SM <sub>Δc40</sub>	TTE-HsdS (wild type)	TTE-HsdM (aa468-507 deletion)

doi:10.1371/journal.pone.0017346.t001

**Table 2.** Data collection and refinement statistics.

A. Data collection statistics		
	Native data	Hg-derivative data
Wavelength (Å)	1.0000	1.5418
Space group	P2 <sub>1</sub> 2 <sub>1</sub> 2 <sub>1</sub>	P2 <sub>1</sub> 2 <sub>1</sub> 2 <sub>1</sub>
Unit cell parameters		
a (Å)	60.966	61.438
b (Å)	137.681	137.747
c (Å)	142.277	142.629
Resolution (Å)	15–1.95 (2.00–1.95)	15–2.25 (2.30–2.25)
No. unique reflections	87,188	58,230
Redundancy	14.4 (14.0)	13.2 (12.6)
R <sub>merge</sub> (%)	5.0 (35.6)	8.4 (48.4)
Completeness (%)	99.9 (100.0)	99.9 (99.6)
I/σ (I)	58.3 (8.5)	27.8 (5.3)
B. Refinement statistics		
Resolution (Å)	10–1.95	
R <sub>work</sub> (%)	19.8	
R <sub>free</sub> (%)	23.8	
Non-hydrogen atoms		
Protein	6193	
Water	786	
Ligand	75	
r.m.s.d. from ideal		
Bonds length (Å)	0.010	
Bond angles (°)	1.25	
Overall average B factor (Å <sup>2</sup> )	36.6	
Ramachandran plot		
Most favored regions (%)	89.9	
Allowed regions (%)	10.1	
Generously allowed regions (%)	0	
Disallowed regions (%)	0	

doi:10.1371/journal.pone.0017346.t002

## Structure determination and refinement

Six mercury sites in each asymmetric unit were determined using SHELXD [21]. After refinement of the heavy atom parameters, the first density map was obtained by SAD phasing using SHARP [22]. Model building was performed with ARP/wARP [23] and COOT [24] at 1.95 Å resolution. Model refinement was performed in CNS [25], and COOT was used for inspection and manual improvement of the model. Within the resolution range of 10–1.95 Å, the native structure was refined to a final  $R_{\text{work}} = 19.8\%$  and  $R_{\text{free}} = 23.8\%$ . Acceptable stereochemistry was confirmed from a Ramachandran plot calculated by PROCHECK [26]. The final model consists of two TTE-HsdS monomers in the asymmetric unit. Residues 327–334 from both subunits are missing. The statistics of the refinement and stereochemistry of the final model are summarized in **Table 2**. The coordinates and structure factors of TTE-HsdS were deposited into RCSB Protein Data Bank with accession code 3OKG.

## DNA binding assay

A non-radioactive electrophoretic mobility shift assay (EMSA) method was used to inspect the DNA binding properties of wild type and mutant TTE-M<sub>2</sub>S<sub>1</sub> complexes. Linear DNA used in the experiments was from the vector pGEX6p-1 digested with *EcoRI* and *NcoI*. The reaction mixture contained 10 mM HEPES at pH 7.0, 300 mM NaCl, 5% glycerol, 1 mM DTT, linear DNA and TTE-M<sub>2</sub>S<sub>1</sub> (wild type or mutant). The samples were subjected to agarose gel electrophoresis after 1 h incubation at 20°C.

## Results

### Overall structure of TTE-HsdS

The crystal structure of TTE-HsdS was determined to 1.95 Å resolution by the single wavelength anomalous diffraction method using a mercury derivative (**Table 2**). The monomer structure, containing 398 amino acids, showed four distinct and continuous

structural regions: the N-terminal TRD (TRD1, Met1 - Pro159), the central CR (CR1, Leu160 - Phe203), the central TRD (TRD2, Pro204–Pro350) and the C-terminal CR (CR2, Leu351–Leu398) (**Figure 1A**). The overall structure obtained for TTE-HsdS confirmed the expected cyclic topology of the subunit [27].

TRD1 and TRD2 exhibited very similar folds. The three-dimensional structural comparison *Z* score of the two globular domains given by the DALI PAIRWISE COMPARISON SERVER [28] were 11.1, giving a root mean square deviation (rmsd) of 2.2 Å for 138 structurally equivalent C $\alpha$  atoms. A 2-stranded antiparallel  $\beta$ -sheet was found at the beginning and end of each TRD ( $\beta$ 1 and  $\beta$ 9 in TRD1,  $\beta$ 10 and  $\beta$ 18 in TRD2). The core structure of each TRD consisted of three  $\alpha$ -helices and two  $\beta$ -sheets with four and three short strands respectively ( $\beta$ 2- $\beta$ 3- $\beta$ 4- $\beta$ 7 and  $\beta$ 5- $\beta$ 6- $\beta$ 8 in TRD1,  $\beta$ 11- $\beta$ 14- $\beta$ 15- $\beta$ 17 and  $\beta$ 12- $\beta$ 13- $\beta$ 16 in TRD2) (**Figure 1A**).

In TTE-HsdS, the CRs were found to be composed of two long antiparallel  $\alpha$ -helices, forming a coiled coils motif. The two helices were held together mainly by hydrophobic interactions and four hydrogen bonds (**Figure S1**). A three amino acid loop (Gln375–Glu377) is inserted in the CR2  $\alpha$ -helice. And there is a fifty degree bend in CR2. The angle and distance between TRD1 and TRD2 indicated the open-form domain-orientation of TTE-HsdS (**Figure 1A**).

### Open form conformation of TTE-HsdS

Superposition of the overall structure of TTE-HsdS and two other HsdS subunits (Mja-HsdS and Mge-HsdS) using the DALI PAIRWISE COMPARISON SERVER gave an rmsd of 8.1 Å for 360 structurally equivalent C $\alpha$  atoms and 11.1 Å for 321 structurally equivalent C $\alpha$  atoms (**Figure S2A**). When only the TRDs were superimposed, the following rmsd values were obtained: 3.7 Å for 146 equivalent C $\alpha$  atoms (TRD1s of TTE-HsdS and Mja-HsdS), 3.9 Å for 117 equivalent C $\alpha$  atoms (TRD1s of TTE-HsdS and Mge-HsdS) (**Figure S2B**), 2.1 Å for 124 equivalent C $\alpha$  atoms (TRD2s of TTE-HsdS and Mja-HsdS) and

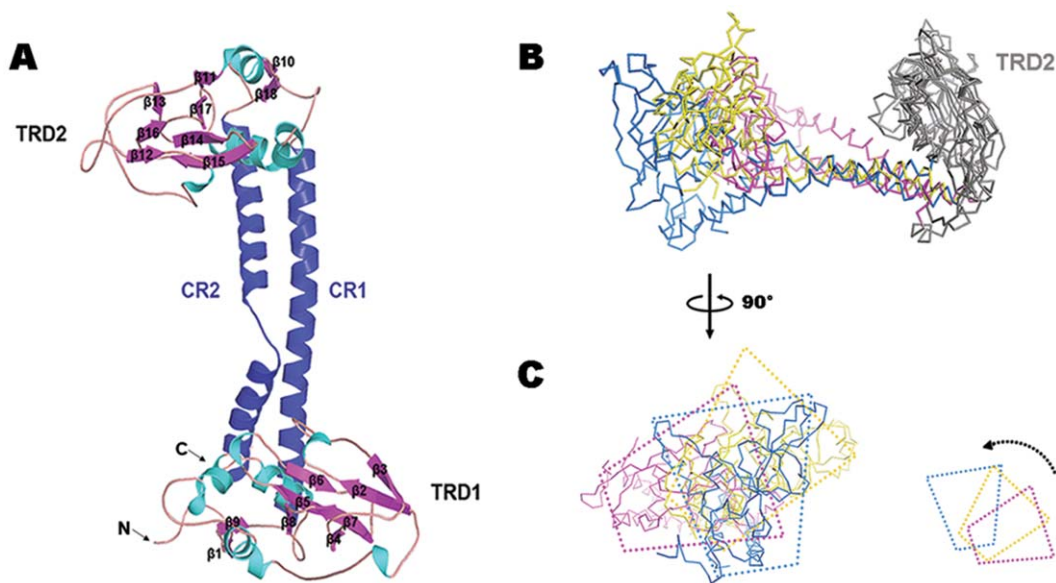


**Figure 1. Overall structure of TTE-HsdS and structural superimposition.** (A) The monomer fold of TTE-HsdS, revealing a cyclical organization of HsdS subunit.  $\alpha$ -helices,  $\beta$ -sheets, and loops in TRDs are colored cyan, magenta, and light pink, respectively. The CRs are colored blue. (B) Superimposition on TRD2 (gray) of TTE-HsdS (blue), Mja-HsdS (yellow) and Mge-HsdS (red). Comparing with Mja-HsdS and Mge-HsdS, the angle and distance between TRD1 and TRD2 of TTE-HsdS are obviously enlarged. (C) The side view of (B). The trapezia indicate the clear differences in domain orientation of TRD1s.

doi:10.1371/journal.pone.0017346.g001

2.9 Å for 123 equivalent C $\alpha$  atoms (TRD2s of TTE-HsdS and Mge-HsdS) (**Figure S2C**). Although both TRD1 and TRD2 have similar folds in the three HsdS subunits, the overall domain orientation is quite different. Hence, significant domain motion could happen within the HsdS subunit. However, the intrasubunit conformational changes are not well understood. By superimposing the TRD2s of the three HsdS subunits, differences between the TTE-HsdS and the other two HsdS subunits could be described in three ways. Firstly, significant bending and twisting of the CRs occurs within TTE-HsdS, giving rotations of 23.7° and 33.8° when compared to Mja-HsdS and Mge-HsdS (**Figure 1B**). Secondly, the angle and distance between TRD1 and TRD2 in TTE-HsdS is larger than in Mja-HsdS and Mge-HsdS (**Figure 1B**). Thirdly, there is an obvious rotation of TRD1 with respect to TRD2 in TTE-HsdS versus the other two HsdS subunits (**Figure 1C**). By superimposing the CRs of the three HsdS subunits, significant conformational differences are also found in CR2s and TRDs (**Figure S3**). Comparisons among the above structures revealed that the TTE-HsdS subunit is in a relatively open conformation. The proposed HsdS-HsdM interaction sites are located in the connection region of CRs and TRDs

and in a helix-loop region in TRDs [10,13]. Domain motion of HsdS subunits would induce a corresponding movement of HsdM subunits. As a result, the M<sub>2</sub>S<sub>1</sub> complex is able to undergo conformational changes.

#### Potential open state of M<sub>2</sub>S<sub>1</sub> complex

Stable M<sub>2</sub>S<sub>1</sub> complexes were purified by co-expression of TTE-HsdS and TTE-HsdM in *E.coli*. Expression of TTE-HsdM alone was insoluble. The molecular weight of the protein complex was determined by analytical ultracentrifugation to be 165 kDa, indicating that the protein complex consists of two HsdM subunits (MW: 58.5 kDa) and one HsdS subunit (MW: 46.5 kDa) (**Figure S4**). The open form conformation structure of TTE-HsdS and the closed state model of M.EcoKI-M<sub>2</sub>S<sub>1</sub> complex (**Figure 2A, C**) were used to construct the open state model of the M<sub>2</sub>S<sub>1</sub> complex. By means of superimposition and replacement of TRDs, we replaced EcoKI-HsdS in the M.EcoKI-M<sub>2</sub>S<sub>1</sub> model with TTE-HsdS to generate the model of TTE-M<sub>2</sub>S<sub>1</sub> (one TTE-HsdS and two EcoKI-HsdM) (**Figure 2B, D and Figure S5**). As expected, the TTE-M<sub>2</sub>S<sub>1</sub> model revealed a completely different open state conformation than the M.EcoKI-M<sub>2</sub>S<sub>1</sub> model. In addition, the

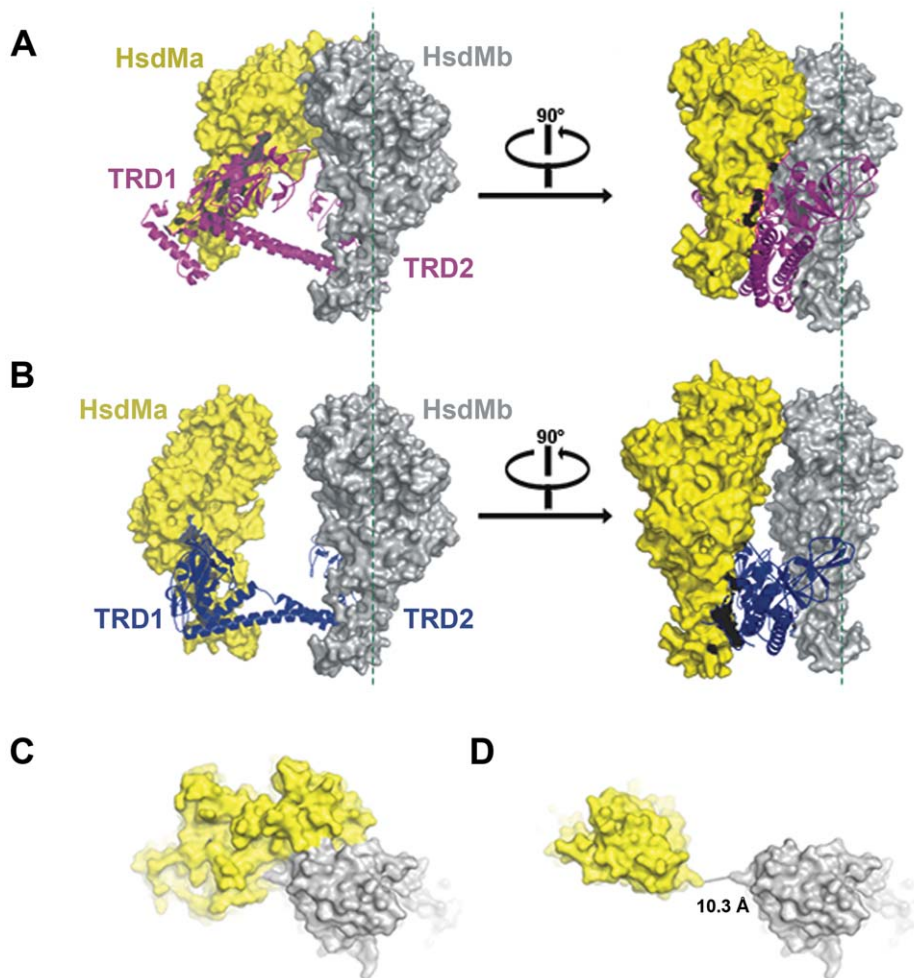


**Figure 2. Models of M<sub>2</sub>S<sub>1</sub> in Closed state and open state.** (A) The closed state model of M.EcoKI-M<sub>2</sub>S<sub>1</sub>, showing the HsdM-HsdM interaction via their N-terminal domains. HsdS is shown as a red ribbon. The two HsdMs (in yellow and gray) are shown as surface. (B) The open state model of TTE-M<sub>2</sub>S<sub>1</sub>. Significant bending and twisting occurs in the CRs, moving the N-terminal domains of HsdMs apart. HsdS is shown as a blue ribbon. The two HsdMs (in yellow and gray) are shown as surface. (C) The top view of M.EcoKI-M<sub>2</sub>S<sub>1</sub> closed state model highlighting the interface between the N-terminal domains of HsdMs. (D) The top view of TTE-M<sub>2</sub>S<sub>1</sub> open state model highlighting the separated N-terminal domains of HsdMs. doi:10.1371/journal.pone.0017346.g002

open state TTE-M<sub>2</sub>S<sub>1</sub> model clearly showed that the clamp-like closed state complex converts to the open state by movement of the N-terminal domains of the HsdM subunits. By using the same protocol, crystal structures of Mja-HsdS and Mge-HsdS can not result in a reasonable open form of the M<sub>2</sub>S<sub>1</sub> complex (Figure S6).

### Inter-subunit interactions of TTE-M<sub>2</sub>S<sub>1</sub>

Type I methyltransferase will remain in the closed state when no DNA is entering or leaving the complex [13]. The M.EcoKI-M<sub>2</sub>S<sub>1</sub> EM model shows that the HsdM subunit C-terminal region contacts the HsdS subunit while the N-terminal regions of the HsdM subunits contact each other. A series of mutation assays were designed in order to confirm these proposed contact regions and identify the specific interaction sites. Firstly, we constructed four co-expression vectors consisting of wild type TTE-HsdS and different TTE-HsdM C-terminal deleted mutants (petDUET\_SMAc10, petDUET\_SMAc21, petDUET\_SMAc30 and petDUET\_SMAc40) (Table 1). Further purification experiments showed that TTE-HsdMAc10 (Δ498–507) can form stable complex with wild type TTE-HsdS but TTE-HsdMAc21 (Δ487–507), TTE-HsdMAc30 (Δ478–507) and TTE-HsdMAc40 (Δ468–507) cannot form stable complexes (Figure 3A). Size exclusion chromatography revealed that the complex formed by TTE-

HsdMAc10 and TTE-HsdS has the same subunit composition as the wild type complex (Figure 3B), indicating that the HsdM-HsdS interaction sites are intact in TTE-HsdMAc10. Residues 466–495 in TTE-HsdM are predicted to form an α-helix, while predictions for TTE-HsdMAc21, TTE-HsdMAc30 and TTE-HsdMAc40 lack this secondary structure element. Therefore, the α-helix in the C-terminal region of TTE-HsdM is an important HsdM-HsdS interaction site.

Four co-expression vectors were also constructed of wild type TTE-HsdS with different TTE-HsdM N-terminal deleted mutants (petDUET\_SMAΔn10, petDUET\_SMAΔn30, petDUET\_SMAΔn40 and petDUET\_SMAΔn50) (Table 2). Purification results showed that only TTE-HsdMAΔn10 (Δ1–10) and TTE-HsdMAΔn30 (Δ1–30) can form stable complexes with TTE-HsdS (Figure 3C). Also, the subunit composition of the two mutant complexes is the same as the wild type complex (Figure 3D). These results clearly show that the deletion of residues 1–30 of TTE-HsdM does not affect HsdM-HsdM interactions, but that the additional deletion of residues 30–40 or residues 30–50 will disrupt the interaction (Figure 3C). The secondary structure prediction shows that residues 30–59 in TTE-HsdM form an α-helix. Damage to this α-helix structure, as in the Δ1–40 and Δ1–50 mutants disrupts HsdM-HsdM interactions and undermines the stability of the TTE-M<sub>2</sub>S<sub>1</sub> complex.

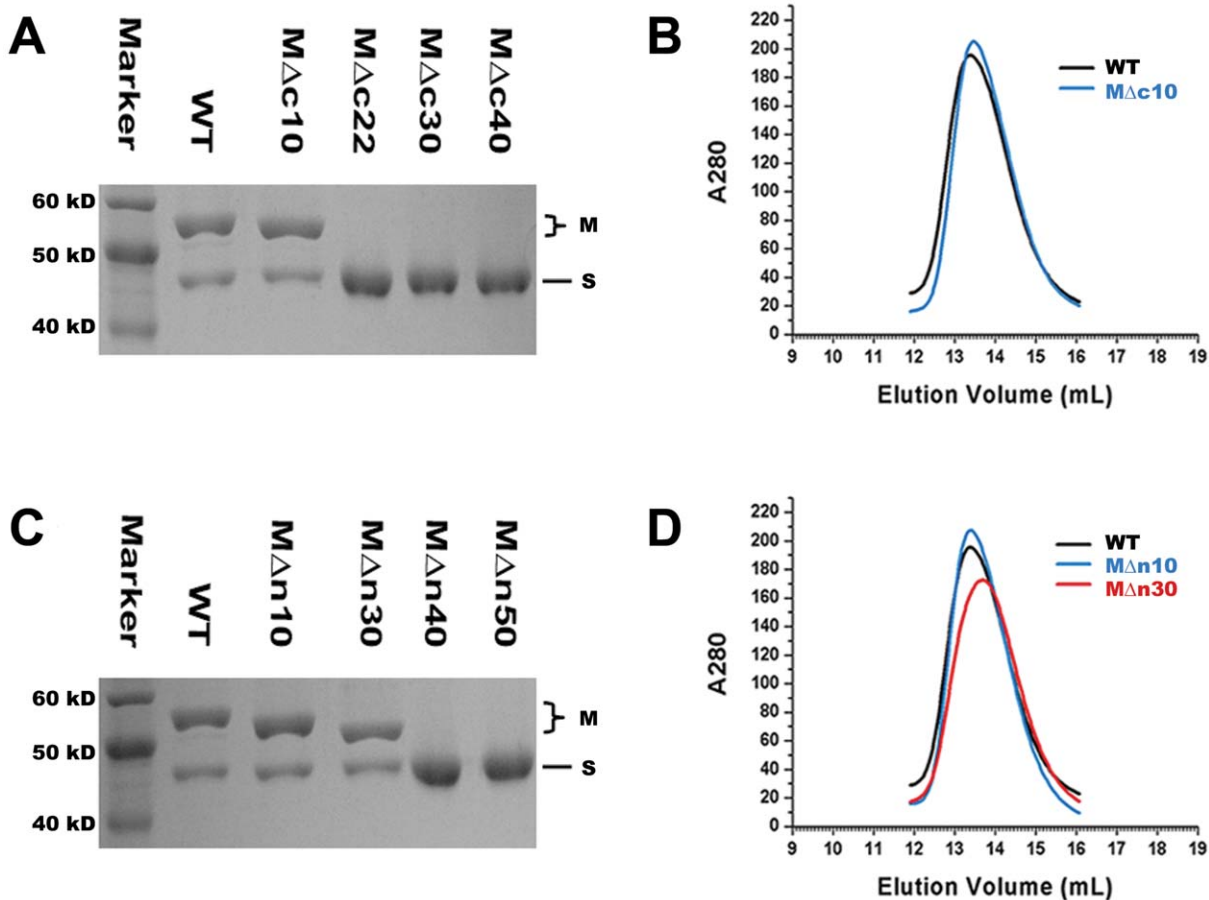


**Figure 3. Mutational assays of TTE-M<sub>2</sub>S<sub>1</sub>.** (A) SDS-PAGE of the co-purification of wild type HsdS and HsdM mutants with C-terminal deletion. Only MΔc10 can be co-purified with HsdS subunit. (B) Gel filtration analysis of TTE-M<sub>2</sub>S<sub>1</sub> and TTE-HsdMAc10<sub>2</sub>S<sub>1</sub>, showing the similar aggregation state between them. (C) SDS-PAGE of the co-purification of wild type HsdS and HsdM mutants with N-terminal deletion. Only MΔn10 and MΔn30 can be co-purified with HsdS subunit. (D) Gel filtration analysis of TTE-M<sub>2</sub>S<sub>1</sub>, TTE-HsdMAΔn10<sub>2</sub>S<sub>1</sub> and TTE-HsdMAΔn30<sub>2</sub>S<sub>1</sub>, showing the similar aggregation state among them.

doi:10.1371/journal.pone.0017346.g003

### Interaction of DNA and TTE-M<sub>2</sub>S<sub>1</sub>

Until now, there has been no DNA binding information for *T. tengcongensis* Type I methyltransferase M<sub>2</sub>S<sub>1</sub> complex. Results of our EMSA assay showed that the mixture of linear vector DNA and wild type TTE-M<sub>2</sub>S<sub>1</sub> was less mobile than free DNA, an effect that was more obvious as the concentration of protein complex was increased (**Figure 4A**). This indicates that TTE-M<sub>2</sub>S<sub>1</sub> can non-specifically bind to linear vector DNA. Unspecific binding with linear DNA is also found with three of the mutant M<sub>2</sub>S<sub>1</sub> complexes (TTE-M $\Delta$ n10<sub>2</sub>S<sub>1</sub>, TTE-M $\Delta$ n30<sub>2</sub>S<sub>1</sub> and TTE-M $\Delta$ c10<sub>2</sub>S<sub>1</sub>). TTE-M $\Delta$ n10<sub>2</sub>S<sub>1</sub> and TTE-M $\Delta$ n30<sub>2</sub>S<sub>1</sub> had similar linear DNA binding affinities as wild type TTE-M<sub>2</sub>S<sub>1</sub> (**Figure 4A**), indicating that the deletion of residues 1–30 from the N-terminal region of TTE-HsdM does not affect the interaction of the

complex with DNA. However, the DNA binding affinity of TTE-M $\Delta$ c10<sub>2</sub>S<sub>1</sub> was weaker than wild type complex DNA binding affinity (**Figure 4A**). This shows the importance of the C-terminal region of the TTE-HsdM subunits for M<sub>2</sub>S<sub>1</sub> complex binding with linear DNA.

In order to identify the TTE-HsdS DNA binding sites, TRD1 and TRD2 were entered into the DALI server [29] to search for structurally related proteins. The search results showed that the DNA binding domain of *TaqI*-Mtase [30] has folds similar to TRD1 and TRD2 with rmsd values of 3.1 Å and 3.2 Å respectively. Putative DNA binding regions in the TRDs were immediately identified from the superposition of the DNA binding domain from *TaqI*-Mtase and the TRDs (**Figure 4B**). Conspicuous sections of positively charged residues are found in the DNA

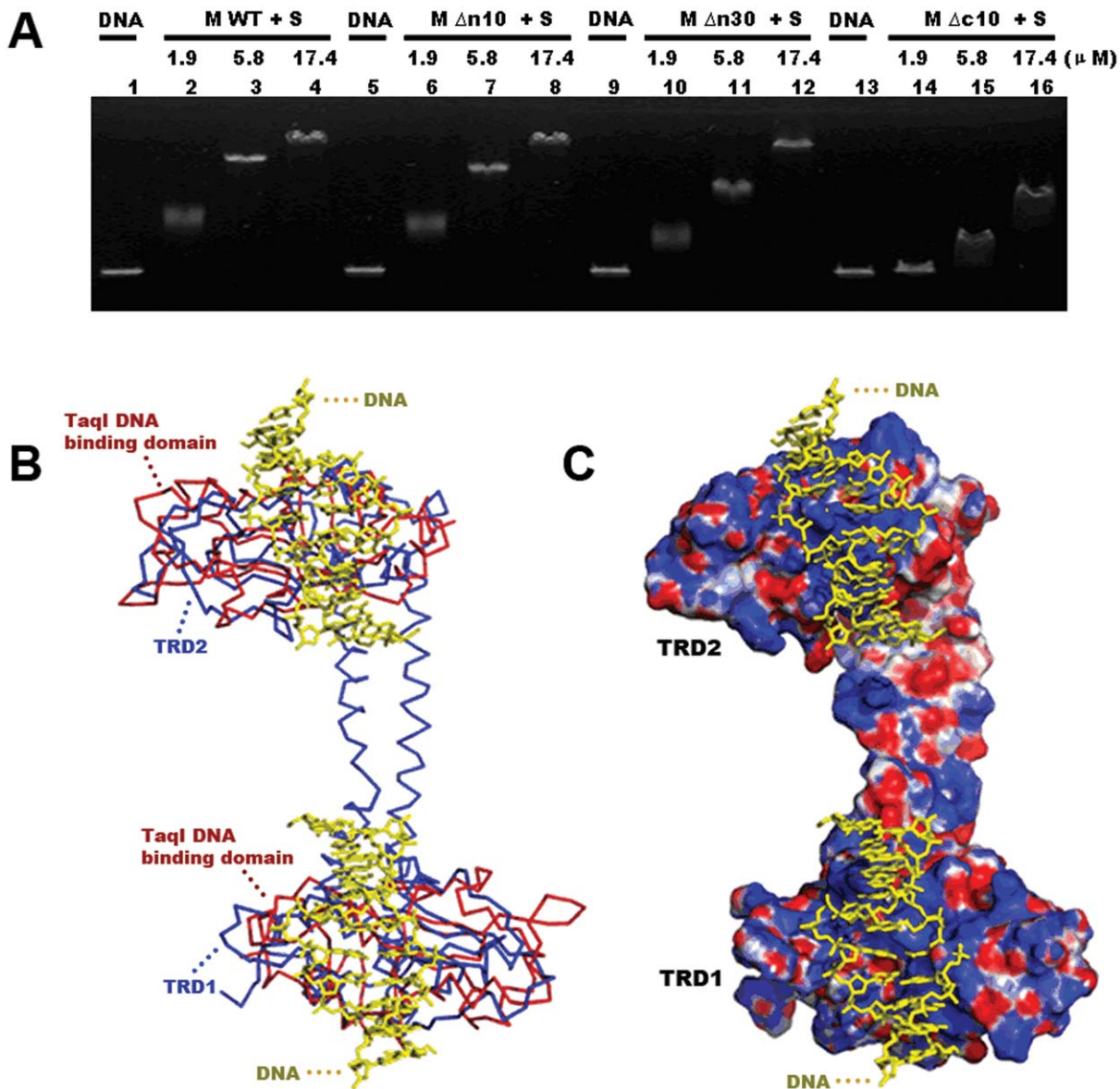


**Figure 4. Interactions of DNA and TTE-M<sub>2</sub>S<sub>1</sub>.** (A) EMSA assays of wild type TTE-M<sub>2</sub>S<sub>1</sub> and its mutants. TTE-M $\Delta$ n10<sub>2</sub>S<sub>1</sub> and TTE-M $\Delta$ n30<sub>2</sub>S<sub>1</sub> have the similar DNA binding affinity with wild type TTE-M<sub>2</sub>S<sub>1</sub>, but the DNA binding affinity of TTE-M $\Delta$ c10<sub>2</sub>S<sub>1</sub> is much weaker. (B) Superposition of the DNA binding domain (red ribbon) of *TaqI* Mtase onto the two TRDs of TTE-HsdS (blue ribbon). The DNA molecules are shown as yellow stick. (C) Electrostatic potential maps of the surface of TTE-HsdS and the DNA binding model. Positive potential is colored blue, neutral potential is colored gray, and negative potential is colored red. doi:10.1371/journal.pone.0017346.g004

binding regions (**Figure 4C**). Through comparison with the DNA binding domain of *TaqI*-Mtase, residues in several equivalent loops of TRDs were found to be involved in DNA binding (TRD1: Asp41-Ser43, Pro64-Arg66, Thr81-Arg82, Ser101-Thr102 and Ser141-Ala144; TRD2: Ser230-Ser233, Gly248-Lys249, Arg280-Ala281, Arg297-Gly298 and Thr332-Asn334), which is consistent with the results of random point mutagenesis studies in EcoKI [31,32].

## Discussion

Compared to the EcoKI-HsdS computational model, significant bending and twisting of the CRs in TTE-HsdS crystal structure enlarges the angle and distance between the TRDs and also shows a small range of rotation between the TRDs. Changes of domain orientation in the HsdS subunit are accompanied by movement of the HsdM subunits that interact with the CRs and TRDs. Interactions of N-terminal domains of the HsdM subunits are also lost. We assume that this series of conformational changes reveals the structural basis mediating the conversion between closed and open states. In our TTE- $M_2S_1$  model, the minimum distance between the N-terminal domains of the two HsdM subunits is about 10.3 Å, which is close to but not sufficient to allow the passage of DNA. Therefore, the TTE- $M_2S_1$  model might reflect an intermediate state which is near to the fully open state. Obviously, this open state model is not very sophisticated for lacking of direct experimental evidence, but it implicates a reasonable picture of the flexible clamp-like enzyme.

Our mutational experiments indicated that  $\alpha$ -helices formed by residues 30–59 and 466–495 of the HsdM subunits are important sites for HsdM-HsdM and HsdM-HsdS interactions, respectively. Damage to either region will disrupt the corresponding interaction and affect assembly of the  $M_2S_1$  complex. However, the N-terminal domains of the HsdM subunits move apart to open the clamp-like complex when DNA is entering or leaving the complex. Target DNA might act as a bridge connecting the N-terminal domains of the HsdM subunits, thereby stabilizing the complex. Therefore, target DNA could facilitate the conversion of the complex from closed to open state.

The computational M.EcoKI- $M_2S_1$  and TTE- $M_2S_1$  models represent the potential closed and open states of type I methyltransferase respectively (Figure 2). These models also indicate that the N-terminal domains of HsdM subunits will move apart from each other during the transition from the closed to open state. According to the results of the EMSA assay and mutational experiments, the target DNA will likely contact the N-terminal domains of the two HsdM subunits to stabilize the complex when DNA is entering or leaving the complex. According to these observations, we speculated a possible “open-close-open” mechanism on the methylation of the target DNA by the  $M_2S_1$  complex. Without DNA binding, the  $M_2S_1$  is in a closed state [13]. But when target DNA is present, the HsdM-HsdM interaction opens to let the DNA in. Then, the  $M_2S_1$  will return to a closed state [13] and the DNA will be methylated. Once the DNA has been methylated, the  $M_2S_1$  complex will transit to an open state to release the target DNA and return to the closed state.

In summary, the crystal structure of TTE-HsdS shows an open form domain-orientation. Conformational differences among TTE-HsdS, Mja-HsdS and Mge-HsdS suggest intra-subunit movements within the HsdS subunit. The structural character of this domain motion was discussed via structural comparison. The potential open state model of the  $M_2S_1$  complex was proposed based on the structure of TTE-HsdS. Combined with the M.EcoKI- $M_2S_1$  closed model, the open state  $M_2S_1$  model reveals

the structural basis of dynamic opening and closing of this clamp-like enzyme. Mutational studies identified two  $\alpha$ -helices in the N- and C-terminal regions of the HsdM subunit that play crucial roles in inter-subunit interactions. In addition, DNA binding assays also showed the importance of the HsdM C-terminal region for DNA binding by the  $M_2S_1$  complex. Based on the work carried out here and in previous studies, we supposed a potential mechanism for the dynamic opening and closing of type I methyltransferase. Notably, many details regarding the hypothesis are still uncertain. More concrete structures and relative investigations are needed for confirmation of this mechanism.

## Supporting Information

**Figure S1 Interactions between the CRs.** Hydrophobic residues are shown in dots model. Residues formed H-bonds (shown in dashes) are shown in stick model.  
(TIF)

**Figure S2 Superimposition of HsdS Structures.** (A) Stereo view of the overall superimposition of the TTE-HsdS (blue), Mja-HsdS (yellow) and Mge-HsdS (red) structures. (B) Stereo view of superimposition of TRD1s. (C) Stereo view of superposition of TRD2s.  
(TIF)

**Figure S3 Superimposition of CRs.** Superimposition of CRs of the TTE-HsdS (blue), Mja-HsdS (yellow) and Mge-HsdS (red) structures.  
(TIF)

**Figure S4 Analytical ultracentrifugation analysis.** The molecular weight of the protein complex was determined to be 165 kD, indicating that the protein complex consists of two TTE-HsdM subunits (MW:58.5 kD) and one TTE-HsdS subunit (MW:46.5 kD).  
(TIF)

**Figure S5 The modeling procedure of TTE- $M_2S_1$ .** EcoKI-HsdS (red) and TTE-HsdS (blue) are shown in cartoon model. HsdM subunits are shown in surface model.  
(TIF)

**Figure S6 The potential states of  $M_2S_1$  complex.** The potential states of  $M_2S_1$  complex based on the conformations of Mge-HsdS (A), Mja-HsdS (B), EcoKI EM model (C) and TTE-HsdS (D). HsdS subunits and HsdM subunits are shown in cartoon model and surface model respectively.  
(TIF)

## Acknowledgments

We thank the staff at Photon Factory, KEK (beamline NW12A, Project No. 2009G188) in Japan, Beijing Synchrotron Radiation Facility (beamline 1W2B) and Shanghai Synchrotron Radiation Facility (beamline BL17U, Project No. 10sr0133) who helped with the data collection. We also thank Xu-Dong Zhao of the IBP core facilities centre for technical support.

## Author Contributions

Conceived and designed the experiments: PG XXY DCL. Performed the experiments: PG QT XMA. Analyzed the data: PG XXY DCL. Contributed reagents/materials/analysis tools: XMA XXY DCL. Wrote the paper: PG XXY DCL.

## References

- Pittard J (1964) Effect of phage-controlled restriction on genetic linkage in bacterial crosses. *J Bacteriol* 87: 1256–1257.
- Bickle TA, Kruger DH (1993) Biology of DNA restriction. *Microbiol Rev* 57: 434–450.
- Roberts RJ, Belfort M, Bestor T, Bhagwat AS, Bickle TA, et al. (2003) A nomenclature for restriction enzymes, DNA methyltransferases, homing endonucleases and their genes. *Nucleic Acids Res* 31: 1805–1812.
- Murray NE (2000) Type I restriction systems: sophisticated molecular machines (a legacy of Bertani and Weigle). *Microbiol Mol Biol Rev* 64: 412–434.
- Redaschi N, Bickle TA (1996) Posttranscriptional regulation of EcoPII and EcoP15I restriction activity. *J Mol Biol* 257: 790–803.
- Calisto BM, Pich OQ, Pinol J, Fita I, Querol E, et al. (2005) Crystal structure of a putative type I restriction-modification S subunit from *Mycoplasma genitalium*. *J Mol Biol* 351: 749–762.
- Obarska A, Blundell A, Feder M, Vejsadova S, Sisakova E, et al. (2006) Structural model for the multisubunit Type IC restriction-modification DNA methyltransferase M.EcoR124I in complex with DNA. *Nucleic Acids Res* 34: 1992–2005.
- Endlich B, Linn S (1985) The DNA restriction endonuclease of *Escherichia coli* B. II. Further studies of the structure of DNA intermediates and products. *J Biol Chem* 260: 5729–5738.
- Szczelkun MD, Dillingham MS, Janscak P, Firman K, Halford SE (1996) Repercussions of DNA tracking by the type IC restriction endonuclease EcoR124I on linear, circular and catenated substrates. *EMBO J* 15: 6335–6347.
- Kim JS, DeGiovanni A, Jancarik J, Adams PD, Yokota H, et al. (2005) Crystal structure of DNA sequence specificity subunit of a type I restriction-modification enzyme and its functional implications. *Proc Natl Acad Sci U S A* 102: 3248–3253.
- Taylor IA, Davis KG, Watts D, Kneale GG (1994) DNA-binding induces a major structural transition in a type I methyltransferase. *EMBO J* 13: 5772–5778.
- Taylor JE, Callow P, Swiderska A, Kneale GG (2009) Structural and functional analysis of the engineered type I DNA methyltransferase EcoR124I(NT). *J Mol Biol* 398: 391–399.
- Kennaway CK, Obarska-Kosinska A, White JH, Tuszyńska I, Cooper LP, et al. (2009) The structure of M.EcoKI Type I DNA methyltransferase with a DNA mimic antirestriction protein. *Nucleic Acids Res* 37: 762–770.
- Cooper LP, Dryden DT (1994) The domains of a type I DNA methyltransferase. Interactions and role in recognition of DNA methylation. *J Mol Biol* 236: 1011–1021.
- Kelleher JE, Daniel AS, Murray NE (1991) Mutations that confer de novo activity upon a maintenance methyltransferase. *J Mol Biol* 221: 431–440.
- Dryden DT, Cooper LP, Murray NE (1993) Purification and characterization of the methyltransferase from the type I restriction and modification system of *Escherichia coli* K12. *J Biol Chem* 268: 13228–13236.
- Abadjieva A, Webb M, Patel J, Zinkevich V, Firman K (1994) Deletions within the DNA recognition subunit of M.EcoR124I that identify a region involved in protein-protein interactions between HsdS and HsdM. *J Mol Biol* 241: 35–43.
- Bao Q, Tian Y, Li W, Xu Z, Xuan Z, et al. (2002) A complete sequence of the *T. tengcongensis* genome. *Genome Res* 12: 689–700.
- Chang Q, Yan XX, Gu SY, Liu JF, Liang DC (2008) Crystal structure of human phosphomevalonate kinase at 1.8 Å resolution. *Proteins* 73: 254–258.
- Otwinowski Z, Minor W (1997) Processing of X-ray diffraction data collected in oscillation mode. *Methods Enzymol* 276: 307–326.
- Sheldrick GM. Experimental phasing with SHELXC/D/E: combining chain tracing with density modification. *Acta Crystallogr D Biol Crystallogr* 66: 479–485.
- Vonrhein C, Blanc E, Roversi P, Bricogne G (2007) Automated structure solution with autoSHARP. *Methods Mol Biol* 364: 215–230.
- Perrakis A, Morris R, Lamzin VS (1999) Automated protein model building combined with iterative structure refinement. *Nat Struct Biol* 6: 458–463.
- Emsley P, Cowtan K (2004) Coot: model-building tools for molecular graphics. *Acta Crystallogr D Biol Crystallogr* 60: 2126–2132.
- Brunger AT, Adams PD, Clore GM, DeLano WL, Gros P, et al. (1998) Crystallography & NMR system: A new software suite for macromolecular structure determination. *Acta Crystallogr D Biol Crystallogr* 54: 905–921.
- Laskowski RA, MacArthur MW, Moss DS, Thornton JM (1993) Procheck - a Program to Check the Stereochemical Quality of Protein Structures. *Journal of Applied Crystallography* 26: 283–291.
- Kneale GG (1994) A symmetrical model for the domain structure of type I DNA methyltransferases. *J Mol Biol* 243: 1–5.
- Holm L, Park J (2000) DaliLite workbench for protein structure comparison. *Bioinformatics* 16: 566–567.
- Holm L, Sander C (1993) Protein structure comparison by alignment of distance matrices. *J Mol Biol* 233: 123–138.
- Goedecke K, Pignot M, Goody RS, Scheidig AJ, Weinhold E (2001) Structure of the N6-adenine DNA methyltransferase M.TaqI in complex with DNA and a cofactor analog. *Nat Struct Biol* 8: 121–125.
- O'Neill M, Dryden DT, Murray NE (1998) Localization of a protein-DNA interface by random mutagenesis. *EMBO J* 17: 7118–7127.
- O'Neill M, Powell LM, Murray NE (2001) Target recognition by EcoKI: the recognition domain is robust and restriction-deficiency commonly results from the proteolytic control of enzyme activity. *J Mol Biol* 307: 951–963.